# Rutherford Backscattering to Study the Near-Surface Region of Volatile Liquids and Solids

**Ulrich K. Krieger,[1]* Thomas Huthwelker,[1,2] Christian Daniel,[2] Uwe Weers,[1] Thomas Peter,[1] William A. Lanford[2]**

**Here we describe the use of Rutherford backscattering spectrometry (RBS) to measure quantitative in situ elemental profiles with high depth resolution, online and nondestructively, in volatile substances (liquid and frozen acids, ice). Samples for analysis are held in a chamber with controlled temperature and partial pressures designed to match conditions for aerosols in Earth's atmosphere. This technique is demonstrated in studies of water solubility in sulfuric acid, hydrochloric acid (HCl) on ice surfaces, the formation of a HCl-hexahydrate surface layer on evaporating HCl-doped ice, and the diffusion of water through this layer.**

The composition of liquid and solid aerosols has been studied by measuring changes in the gas flowing over model systems. Such a mass spectrometry–based approach leaves the very nature of the uptake mechanisms inside the condensed phase unexplored. Measurement of elemental or isotopic concentration profiles below the surface of volatile materials would provide key data for understanding the microscopic mechanism underlying their physical chemistry. However, such measurements present a substantial analytical challenge (*1*). The central property that distinguishes high vapor pressure solids and liquids is the dynamic nature of their surfaces. For example, ice at –25°C sublimates $\sim 3 \times 10^5$ monolayers/s, as calculated from its vapor pressure. Most modern profiling methods rely on either sputtering or ion energy loss to derive depth information. Sputtering methods cannot be applied to highly volatile samples because of the rapid redistribution that would occur on a freshly sputtered surface. Ion beam analysis might seem incompatible with the high vapor pressures associated with these materials. Here, we demonstrate that a simple modification of a conventional ion beam analysis chamber (*2*) allows these materials to be studied.

Rutherford backscattering spectrometry (RBS) is well described in the literature (*3*), so only a brief overview of RBS is presented here. For measurement of concentration versus depth by RBS, a sample is bombarded with ions (typically 2-MeV $He^+$ ions) and the energy spectrum of backscattered ions is recorded. For a given target composition, the RBS energy spectrum is completely determined by the He ion–target nucleus scattering cross section, by conservation of energy and momentum in elastic scattering, and by the energy loss ($dE/dx$) of $He^+$ ions penetrating the target material. Because of this simple physics, RBS spectra can be quickly and reliably interpreted in terms of target composition.

At a scattering angle of 180°, the energy $E$ of a backscattered ion is

$$E = [(M_1 - M_2)/(M_1 + M_2)]^2\, E_{\mathrm{beam}} \qquad (1)$$

(*3*), where $M_1$ is the mass of the nucleus of the projectile ion, $M_2$ is the mass of the nucleus of the target atom, and $E_{\mathrm{beam}}$ is the energy of the incident projectile ions. For a selected beam energy and mass, measuring the backscattered energy $E$ determines the nuclear mass of the target atom, and hence its atomic number. The probability for such a scattering event is given by the Rutherford Coulomb scattering cross section for a wide range of projectile masses and energies. Hence, a thin target consisting of a series of masses $M_i$ would yield a backscattering energy spectrum with a corresponding series of peaks with energy $E_i$ given by Eq. 1. Measuring the number of events in each mass peak determines the composition of the target.

Usually, targets are thick enough that the incident and backscattered ions lose substantial energy (*4*) as a result of inelastic interaction with the target electrons as they penetrate the target material. In this case, scattering by nuclei residing deeper in the target results in lower backscatter energy than that given by Eq. 1. The depth of this scattering event can be calculated from the tabulated values of the energy loss $dE/dx$ without further calibration. Thus, for thick targets the backscattered energy spectrum is not a series of elemental peaks, but rather a series of elemental steps. The backscatter yield at a specific energy depends on the number of atoms present at a depth corresponding to this energy. Hence, often the raw spectrum can be qualitatively read as a concentration profile, with the highest energy giving the surface concentration and lower energies giving concentrations deeper inside the sample.

Three examples are presented to illustrate the method, the first of which is the uptake of water by $H_2SO_4$. A considerable fraction of the atmospheric aerosol consists of aqueous sulfuric acid droplets, whose surface properties are of great interest for atmospheric chemists. For $H_2SO_4$ targets, a few drops of acid are spread on a fused silica plate (roughened by sandblasting), which sustains a liquid film in a vertical plane for many hours. This target must be kept in an ambient environment with at least a few hundred pascals of water to ensure its long-term stability, because $H_2SO_4$ in dry environments (such as vacuum) slowly decomposes into $H_2O$ and $SO_3$.

Figure 1 shows three overlaid RBS spectra recorded from a liquid sulfuric acid target bombarded with 2-MeV He ions. Spectrum 1 was recorded with the target in relatively dry conditions; spectra 2 and 3 were recorded in more moist environments. As expected, all spectra show elemental steps for S and for O.

The approximate concentration of the corresponding aqueous sulfuric acid solutions can be read directly from the spectra by ratioing heights ($H_S$) for sulfur to the height ($H_O$) for oxygen: $N_S/N_O \cong H_S/H_O(z_O/z_S)^2$, where $z_O$ and $z_S$ are the atomic numbers for S and O, respectively, and $N_S/N_O$ is the ratio of sulfur to oxygen. Using a more complete RBS analysis (*3, 5*) shows that these RBS data are in excellent agreement (within 1.5%) of the solubilities determined by thermodynamic models (*6, 7*) based on vapor pressure measurements.

In addition, analysis of the RBS spectra further shows that the S/O ratio is constant to 1% over the depth range profiled (0 to 6000 Å). This is consistent with Auger experiments (*8*) probing the first few layers below the surface (~20 Å), which show no difference in composition when compared to that of the bulk. However, sum frequency experiments (*9*) show that fewer water molecules (-10%) are present at the very first surface layer, an effect beyond the depth resolution (*4*) of our experiment.

The second example is the study of the transport and location of Cl in ice. Diffusion kinetics and solubility of HCl in ice have been studied by numerous methods. However, the diffusion coefficient for HCl in ice at 185 K varies widely from $D \approx 10^{-5}$ cm²/s (*10, 11*) to $D < 10^{-16}$ cm²/s (*12, 13*). This discrepancy may be attributable to different experimental techniques and/or preparation of ice with different morphologies [polycrystallinity, purity at grain boundaries or at the

---

[1] Institute for Atmospheric and Climate Science, ETH Zürich, Hönggerberg HPP, 8093 Zürich, Switzerland. [2] Physics Department, State University of New York, Albany, NY 12222, USA.

*To whom correspondence should be addressed. E-mail: krieger@atmos.umnw.ethz.ch

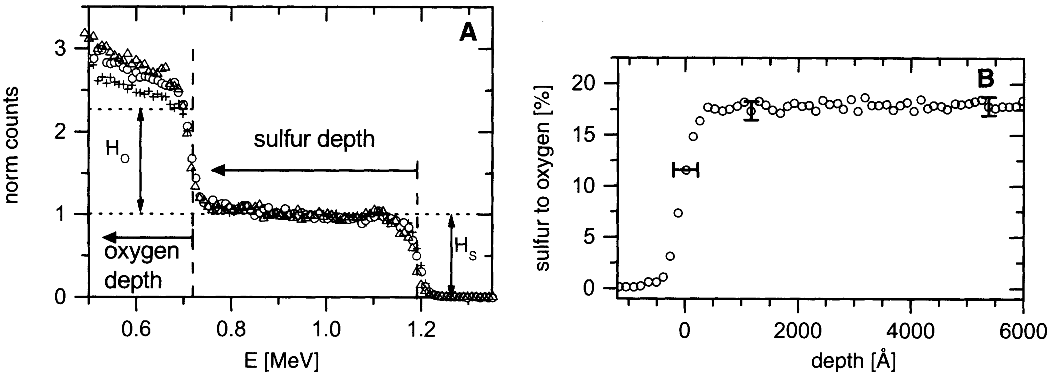

**Fig. 1.** Water solubility in aqueous sulfuric acid at $T = -18°C$. (**A**) Normalized (to sulfur step) RBS spectra of solutions at three different water vapor pressures. Spectrum 1 (crosses): $p_{H_2O} = 0.733$ Pa, composition deduced from spectra $c_{expt} = 77.1$ weight %, composition according to model (*7*) $c_{model} = 77.2$ weight %. Spectrum 2 (circles): $p_{H_2O} = 4.38$ Pa, $c_{expt} = 69.6$ weight %, $c_{model} = 69.5$ weight %. Spectrum 3 (triangles): $p_{H_2O} = 11.8$ Pa, $c_{expt} = 64.6$ weight %, $c_{model} = 63.3$ weight %. (**B**) Spectrum 1 converted to concentration (ratio of atomic sulfur to atomic oxygen) versus depth. Error bar in depth was estimated from detector resolution and scattering geometry (*4*); error bar in concentration was estimated from counting statistics.

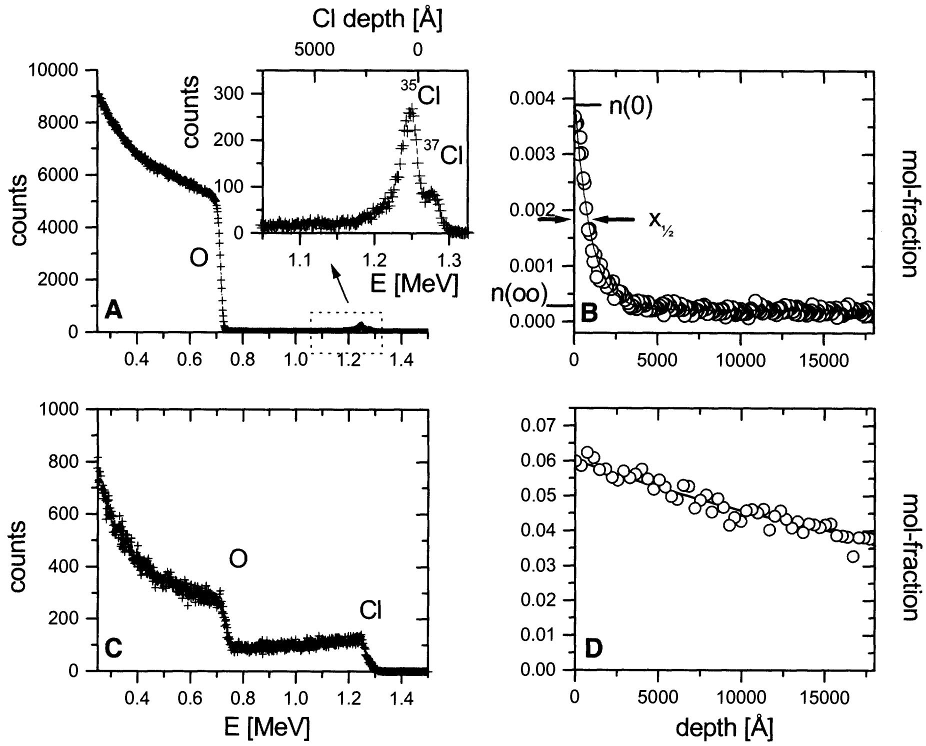

**Fig. 2.** (**A**) RBS spectra of HCl-doped ice, sample prepared from 0.022 mol % HCl solution probed at 195 K; the inset shows an enlargement of the spectra in the Cl region. (**B**) Mole fraction of HCl versus depth converted from spectrum in (A). (**C**) RBS spectrum of a sample made from a 5.4 mol % HCl solution and probed at 205 K. (**D**) Corresponding depth profile.

junctions where three grains meet (triple junctions), and porosity]. Using RBS for direct measurement of the chlorine diffusion profile in ice allows a direct measurement of both solubility and diffusivity.

Polycrystalline ice targets containing Cl were prepared by immersing the cooled sample holder into a water-HCl solution (*14*). The ice sample was then evaporated through a pinhole of known size, allowing calculation of the evaporation rate. Because of the finite solubility (Henry's law constant $H = n_{ice}/n_{gas}$) and diffusivity ($D$) of HCl in ice, a steady-state HCl concentration profile forms near the ice surface. Given that the ice surface is moving with a known velocity $c$ (due to evaporation), this profile can be modeled as

$$n(x) = n(\infty) + 4cH\,n(\infty)\exp(-cx/D)/v_{gas} \qquad (2)$$

where $n(x)$ is number density of chloride ions at distance $x$ from the surface, and $v_{gas}$ is the velocity of the HCl molecules in the gas phase (*15*).

Figure 2 shows RBS spectra and deduced Cl profiles for samples prepared under two different conditions. Figure 2A shows a spectrum from a sample held at 195 K made from a dilute HCl solution. The dominant feature in the RBS spectrum is backscattering from oxygen in the bulk ice. The small peak at ~1.27 MeV originates from scattering from two Cl isotopes, $^{35}$Cl and $^{37}$Cl. Converting this high-energy region of the RBS spectrum into a Cl profile gives the result shown in Fig. 2B. This profile is characterized by a surface peak and a long low-concentration tail extending deep into the ice. Figure 2C shows an RBS spectrum from a sample made from a more concentrated HCl solution. The concentration profile shown in Fig. 2D has the same basic features as that for Fig. 2A, except that the Cl concentration is much greater. It is characterized by a high concentration at the surface, slowly decreasing with depth.

Fits to the data using Eq. 2 are shown as solid lines in Fig. 2, B and D. The diffusion constant obtained from the fit of Fig. 2A is $5 \times 10^{-12}$ cm$^2$/s $< D < 3 \times 10^{-11}$ cm$^2$/s and the Henry's law constant $7 \times 10^{10} < H < 3 \times 10^{11}$, with the uncertainties arising mainly through the uncertainty in determining $c$. The temperature dependence of the diffusion was evaluated between 195 and 220 K, leading to an Arrhenius diffusion activation energy of 14.9 ± 2.5 kcal/mol. These data agree favorably with recent laser desorption depth profiling data (*16*), from which can be deduced a value of $D = 1.1\ (\pm 0.2) \times 10^{-10}$ cm$^2$/s for 194.9 K and an activation energy of 15.3 ± 1.0 kcal/mol.

Application of Eq. 2 to the spectrum shown in Fig. 2, C and D (high-doped ice) yields a diffusion constant of $4 \times 10^{-9}$ cm$^2$/s $< D < 1.6 \times 10^{-8}$ cm$^2$/s. This number is about a factor of 5 to 10 smaller than what is estimated for the diffusivity of HCl in a liquid (*17*). This supports the view that, with increased doping, the triple junctions of polycrystalline ice (*18–20*) containing a liquid HCl solution become dominant for HCl uptake.

The third example involves the formation of HCl hexahydrate ($HCl{\cdot}6H_2O$)–coated ice and its evaporation. The target for this study was a three-layer sample consisting of HCl-doped ice between layers of pure ice mounted on a carbon substrate (*21*). Initially, the target temperature was slowly raised from its deposition temperature until changes were first observed at $T = 185$ K. The sample was then held at this temperature, and backscatter spectra were recorded as a function of time.

Backscatter spectra from the target as it was deposited and at two later times are shown in Fig. 3. The high-energy part of the spectrum reflects the Cl distribution in the sample. The temporal evolution of the target can be summarized as follows:

The initial target composition was (3.2 μm $H_2O$)/(3.2 μm 0.07 molar HCl)/(2.7 μm $H_2O$), as deduced from top spectrum in Fig. 3A. Note that the Cl peak is not located at the surface but below. Also, no carbon signal appears at the surface, which indicates that the sample covers the substrate homogeneously and not as separated islands.

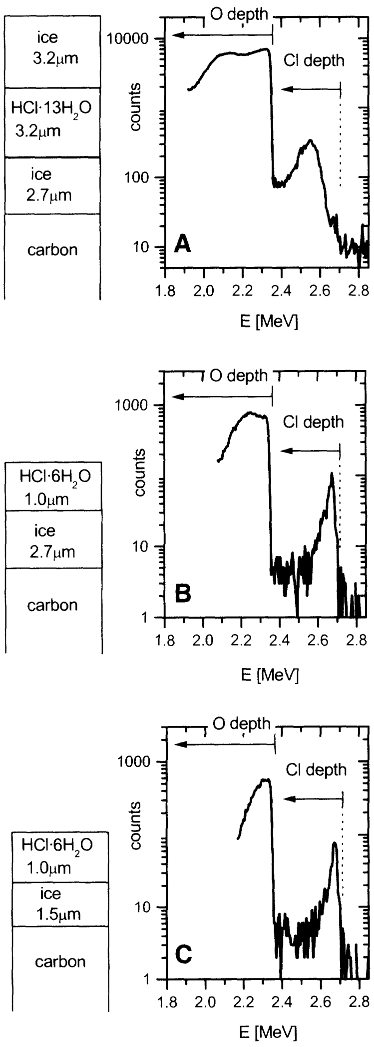

**Fig. 3.** RBS (3-MeV protons) spectra of a sample consisting of a HCl-doped ice layer sandwiched between two ice layers on a carbon substrate held at 185 K and evaporating into vacuum. Note the logarithmic scale of the ordinate. (**A**) The sample at the start of the evaporation. (**B**) The sample after 30 min. (**C**) The sample after 60 min. At the left are sketches of the composition of the sample at the corresponding time, analyzed from the spectra.

The spectrum shown in Fig. 3B was recorded after holding the sample at 185 K for 30 min. The overall ice is thinner as a result of continuous evaporation (see the extent of the O signal). Furthermore, the Cl is now located at the surface at a 1:6 concentration, which is the stoichiometry of the hexahydrate of HCl. This hydrate is known to be stable at this temperature (*22*).

The spectrum in Fig. 3C was recorded after holding the sample at 185 K for 60 min. The hexahydrate remains at the surface, but the thickness of the underlying ice is reduced. Spectra recorded at later times show that eventually the layer of underlying ice completely disappears, and then the hexahydrate evaporates.

The coating of atmospheric ice particles with acid hydrates is a topic of great interest. Coating of ice particles with nitric acid tetrahydrate (NAT) has been proposed as a mechanism enhancing stratospheric denitrification, which strongly influences ozone hole chemistry (*23*, *24*). In our experiment we can compare the evaporation rate (due to the continuous pumping) of the ice at the surface (41 ± 5 Å/s) to that of the ice through the hexahydrate (29 ± 6 Å/s). This hexahydrate layer on top of the ice slows the evaporation rate of ice by only 30% (i.e., it is not a very effective coating). With the use of isotopically labeled water ($^{18}O$, $^{2}H$), it should be possible to study the mechanism of transport of water through the hydrate using nuclear reaction analysis (*25*).

These three examples illustrate that RBS is a practical way to study near-surface chemistry, and that its advantages (rapid, reliable, and quantitative without use of reference standards) still apply even in this context.

### References and Notes

1. High-vacuum techniques used commonly to study surfaces (low-energy electron diffraction, Auger, x-ray photoelectron spectroscopy, etc.) must undergo elaborate modifications in order to be used in water vapor pressures up to $10^{-2}$ Pa (*8*). Techniques based on nonlinear optics (second harmonic generation, sum frequency generation) (*9*) are specific to the outer monolayer of the sample and cannot probe the region below the surface. The same holds true for ion scattering and recoil spectroscopy (*26*) using incident ions with low energies (1 to 5 keV), which is sensitive to the top few Å of a surface.
2. A sample holder is heated under computer control relative to a liquid nitrogen reservoir. This setup can maintain the sample temperature between 140 and 260 K. The target holder is mounted in a chamber with inlet valves for water and trace gases. There is a differential pumping aperture (a 30-cm liquid nitrogen inline trap) between this chamber and the high vacuum of the accelerator beamline. Water pressures can be maintained between $10^{-3}$ Pa and 300 Pa. The absolute pressure and gas composition in the cell are continuously measured by a Baratron gauge and by mass spectroscopy, respectively. A conventional Si charged-particle detector is mounted within the cell to measure the energy spectra of ions backscattered from the target. Detectors have been used at water pressures up to a few hundred Pa and HCl pressures up to $10^{-2}$ Pa. No ill effects from these environments on the Si detector have been observed.
3. W.-K. Chu, J. M. Mayer, M.-A. Nicolet, *Backscattering Spectrometry* (Academic Press, New York, 1978).
4. The energy loss *dE*/*dx* of an incident ion depends on the identity of the projectile ion, its energy, and the elemental composition and density of the target (*3*). For the sulfuric acid solution of Fig. 1B probed with 2-MeV He ions, this energy loss is 21.4 eV/Å (*3*). Because the energy resolution of our detector is about 13 keV, the theoretical limit for the depth resolution in experiments with normal incidence is 610 Å. However, we used a scattering geometry with the target tilted by 45°, leading to a limit of 430 Å. The full width at half-maximum of the derivative of the concentration profile of Fig. 1B is 500 Å, consistent with these estimations, because the finite detector size lowers the resolution.
5. L. R. Doolittle, *Nucl. Instrum. Methods* **B9**, 344 (1985).
6. A. Tabazadeh, R. P. Turco, M. Z. Jacobson, *J. Geophys. Res.* **99**, 12897 (1994).
7. K. S. Carslaw, S. L. Clegg, P. Brimblecombe, *J. Phys. Chem.* **99**, 11557 (1995).
8. D. H. Fairbrother, H. Johnston, G. Somorjai, *J. Phys. Chem.* **100**, 13696 (1996).
9. C. Radüge, V. Pflumio, Y. R. Shen, *Chem. Phys. Lett.* **274**, 140 (1997).
10. M. J. Molina, T.-L. Tso, L. T. Molina, F. C.-Y. Wang, *Science* **238**, 1253 (1987).
11. Such high values for *D* up to $10^{-5}$ $cm^2/s$ are representative of HCl diffusing through a melted ice surface, which arose from high partial pressures of HCl (*27*).
12. F. Dominé, E. Thibert, F. van Landeghem, E. Silvante, P. Wagnon, *Geophys. Res. Lett.* **21**, 601 (1994).
13. Often the diffusion constant has been measured at higher temperatures and extrapolated to 185 K; see the discussion in (*28*).
14. After a thin (~mm) ice film formed, the sample holder was transferred into the analysis cell and evacuated. During these measurements, the sample temperature was controlled and the cell was continuously pumped (with no water inlet).
15. V. G. Smith, W. A. Tiller, J. W. Rutter, *Can. J. Phys.* **33**, 723 (1955).
16. F. E. Livingston, S. M. George, *J. Phys. Chem. A* **105**, 5155 (2001).
17. B. P. Luo, S. L. Clegg, Th. Peter, R. Müller, P. J. Crutzen, *Geophys. Res. Lett.* **21**, 49 (1994).
18. E. W. Wolff, R. Mulvaney, *Geophys. Res. Lett.* **16**, 487 (1989).
19. R. Mulvaney, E. W. Wolff, *Nature* **331**, 247 (1988).
20. J. F. Nye, in *Physics and Chemistry of Ice*, N. Maeno, T. Hondoh, Eds. (Hokkaido Univ. Press, Sapporo, Japan, 1992), pp. 200–205.
21. This target was made by bleeding gas (water or HCl-water) into the target chamber with the substrate at liquid nitrogen temperature. After deposition, this three-layer target was held in the analysis chamber, the chamber was continuously pumped (with no water inlet), and its composition was monitored with the ion beam. Because this target was thicker than can be probed using the 2-MeV He RBS, an analyzing beam of 3-MeV protons was used.
22. G. Vuillard, *C. R. Acad. Sci.* **241**, 1308 (1955).
23. S. C. Wofsy *et al.*, *Geophys. Res. Lett.* **17**, 449 (1990).
24. T. Peter, R. Müller, P. J. Crutzen, T. Deshler, *Geophys. Res. Lett.* **21**, 1331 (1994).
25. J. R. Tesmer, M. Nastasi, Eds., *Handbook for Modern Ion Beam Analysis* (Material Research Society, Pittsburgh, PA, 1995).
26. M. Tassotto, T. J. Gannon, P. R. Watson, *J. Chem. Phys.* **107**, 8899 (1997).
27. J. P. D. Abbatt *et al.*, *J. Geophys. Res.* **97**, 15819 (1992).
28. F. Dominé, I. Xueref, *Anal. Chem.* **73**, 4348 (2001).
29. We thank A. Haberl and W. Skala for technical support with the Dynamitron accelerator at SUNY Albany. Parts of the work were performed at the Max Planck Institute for Chemistry, Mainz, Germany, and supported by the Federal Ministry of Education and Research, Germany, under contract AFS 07AF207/3.

28 September 2001; accepted 9 January 2002